

AD-A242 572



REPORT DOCUMENTATION PAGE

2

E
391
D

2b. DECLASSIFICATION / DOWNGRADING SCHEDULE		1b. RESTRICTIVE MARKINGS	
4. PERFORMING ORGANIZATION REPORT NUMBER(S) Report # 4		3. DISTRIBUTION / AVAILABILITY OF REPORT Approved for public release; distribution unlimited.	
6a. NAME OF PERFORMING ORGANIZATION Washington University	6b. OFFICE SYMBOL (if applicable)	7a. NAME OF MONITORING ORGANIZATION Office of Naval Research	
6c. ADDRESS (City, State, and ZIP Code) One Brookings Drive St. Louis, MO 63130-4899		7b. ADDRESS (City, State, and ZIP Code) 800 N. Quincy Street Arlington, VA 22217-5000	
8a. NAME OF FUNDING / SPONSORING ORGANIZATION ONR	8b. OFFICE SYMBOL (if applicable)	9. PROCUREMENT INSTRUMENT IDENTIFICATION NUMBER N00014-90-J-4118; R&T Code (413M001)	
8c. ADDRESS (City, State, and ZIP Code) 800 N. Quincy Street Arlington, VA 22217-5000		10. SOURCE OF FUNDING NUMBERS	
		PROGRAM ELEMENT NO.	PROJECT NO.
		TASK NO.	WORK UNIT ACCESSION NO.
11. TITLE (Include Security Classification) Direct Electron-to-Carbon Polarization Transfer in Homogeneously Doped Polycarbonates			
12. PERSONAL AUTHOR(S) Mobae Afeworki, Shimon Vega, and Jacob Schaefer			
13a. TYPE OF REPORT Technical	13b. TIME COVERED FROM TO	14. DATE OF REPORT (Year, Month, Day) 11/14/91	15. PAGE COUNT 32
16. SUPPLEMENTARY NOTATION			
17. COSATI CODES		18. SUBJECT TERMS (Continue on reverse if necessary and identify by block number)	
FIELD	GROUP	SUB-GROUP	
		DNP; polycarbonate; sideband patterns; molecular motion.	
19. ABSTRACT (Continue on reverse if necessary and identify by block number)			
A direct-electron-to-carbon DNP solid-effect polarization transfer is observed for the aromatic and carbonyl carbons of polycarbonate homogeneously doped with BDPA. The direct electron-to-carbon polarization transfer operates over a range of 30 to 60 Å. Carbons that are closest to the free radicals are polarized first and have the longest spin-lattice relaxation times. Fourier transforms of time-domain magnetization, synchronously detected under combined chemical shift and C-H dipolar interactions, show an asymmetrical sideband pattern in the dipolar frequency dimension. Simulations that qualitatively agree with the observed asymmetrical sideband patterns are obtained by assuming that molecular motion in the vicinity of the bulky free radical is reduced.			
20. DISTRIBUTION / AVAILABILITY OF ABSTRACT <input checked="" type="checkbox"/> UNCLASSIFIED/UNLIMITED <input type="checkbox"/> SAME AS RPT. <input type="checkbox"/> DTIC USERS		21. ABSTRACT SECURITY CLASSIFICATION	
22a. NAME OF RESPONSIBLE INDIVIDUAL Dr. Jacob Schaefer		22b. TELEPHONE (Include Area Code) 314-935-6844	22c. OFFICE SYMBOL

IV. Direct Electron-to-Carbon Polarization Transfer in Homogeneously Doped Polycarbonates

Mobae Afeworki†, Shimon Vega*, and Jacob Schaefer

Department of Chemistry
Washington University
St Louis, MO 63130

Accession For	
NCIS GRAB	<input checked="" type="checkbox"/>
DTIC TAB	<input type="checkbox"/>
Unannounced	<input type="checkbox"/>
Justification	
By _____	
Distribution/	
Availability Codes	
Dist	Avail and/or Special
A-1	



†Present Address: Exxon Research and Engineering Company, Annandale, NJ 08801

*Permanent Address: Department of Chemical Physics, The Weizmann Institute of Science, Rehovot 76100, Israel.

91-15774

ABSTRACT

A direct electron-to-carbon DNP solid-effect polarization transfer is observed for the aromatic and carbonyl carbons of polycarbonate homogeneously doped with BDPA (see previous papers for notation). The direct electron-to-carbon polarization transfer operates over a range of 30 to 60 Å. Carbons that are closest to the free radicals are polarized first and have the longest spin-lattice relaxation times. Fourier transforms of time-domain magnetization, synchronously detected under combined chemical-shift and C-H dipolar interactions, show an asymmetrical sideband pattern in the dipolar frequency dimension. Simulations that *qualitatively* agree with the observed asymmetrical sideband patterns are obtained by assuming that molecular motion in the vicinity of the bulky free radical is reduced.

INTRODUCTION

Attempts to transfer polarization from electrons in doped PS across an interface directly to carbons in undoped PC in thin-film PC/PS blends failed (1). In this paper, we discuss successful direct *electron-to-carbon* DNP polarization transfers in homogeneously doped polycarbonates. To monitor the DNP-generated carbon magnetization, synchronous sampling was performed as the carbon magnetization evolved under chemical-shift interactions only, and under combined chemical-shift and C-H dipolar interactions. In the latter situation, the H-H interactions were suppressed by multiple-pulse decoupling. This scheme has an advantage over the DRSE

technique of III by eliminating the two-rotor-period delay during which electron flips can dephase carbon magnetization. Results obtained from direct electron-to-carbon polarization transfers can be related to electron-carbon distances in the glassy solid state.

EXPERIMENTS

DNPFT: The DNPFT pulse sequence is an alternate-block, equal-heat, add-subtract pulse sequence with all relaxation delays exactly balanced in the two halves of the experiment. (For a similar sequence, see Figure 5 in I). The first half starts with a variable period of microwave irradiation at the difference of the *electron and carbon* Larmor frequencies followed by a 90° inspection pulse on the carbon channel. In the second half of the experiment, the microwave irradiation is delayed until after data acquisition. In both halves, the ¹³C signal detection begins immediately after the ¹³C 90° inspection pulse. Protons are decoupled throughout the experiment except during the microwave-irradiation periods. The ¹³C 90° inspection pulse is cycled through all four phases. A 180° ¹³C inversion followed by a recovery delay can be placed before the inspection pulse to measure spin-lattice relaxation times of DNP-enhanced carbon signals.

DNPFT-echo: This experiment is similar to the DNPFT experiment just described except the ¹³C signal is detected as an echo two rotor periods after the ¹³C inspection pulse. A 180° pulse at the end of the first rotor period refocuses chemical shifts. Microwave irradiation is applied before the ¹³C inspection pulse in the first half of the experiment, and after data

acquisition in the second half. Protons are decoupled except during the microwave-irradiation periods.

Synchronous Detection: Data sampling in the DNPFT and DNPFT-echo experiments was sometimes synchronized with the rotor period. For a spinning speed of 1859 Hz, sixteen one-point detections separated by 33.6 μ s exactly fit into one rotor period. The synchronous detection is performed in one of two ways (Figure 1). Carbon evolution is observed either under chemical-shift interactions only (C-H dipolar interactions decoupled), or under combined chemical-shift and C-H dipolar interactions (with H-H interactions decoupled by a semi-windowless MREV-8 multiple-pulse decoupling). The cycle time of the MREV-8 sequence and the one-point detections are matched, with rotational echoes forming every 16th data point. A variation in the synchronous-sampling experiment involved delaying the H-H multiple-pulse decoupling before the start of the synchronous data acquisition by an integral number of rotor periods during which the C-H interactions are decoupled (Figure 2).

The first few data points in the synchronous-sampling experiment were collected before complete recovery of the spectrometer from the ^{13}C inspection pulse. If the time-domain data were to be analyzed directly without Fourier transforms, the first five points only were left shifted and the data analysis was done by comparing the formation and decay of the first few echoes. Sometimes a 16-point left shift was performed; the data analysis therefore started at the top of the first echo. The 16-point left shift was followed by zero filling to 1-K data points and Fourier transformation with a 20-Hz line broadening. The resulting spectra are referred to as complete Fourier transforms. In some cases, as for instance

in using the delayed H-H multiple-pulse decoupling of Figure 2, the data analysis was done by a Fourier transform of the second set of 16 time-domain points only, to obtain a 16-point absorption-mode frequency spectrum.

Simulations: Theoretical results were obtained by numerical calculations using a computer program [1] constructed to simulate NMR signals under a variety of interactions and magic-angle spinning speeds on a two-spin system (both spin one-half). The interactions included chemical shift *only*, and chemical shift *plus* C-H dipolar, with no H-H interactions. The calculations were modified to include two-site jumps that simulated the π flips of the phenyl rings of polycarbonate.

RESULTS

DNPFT: The ^{13}C DNP-difference signals for PC(*) (Figure 3, top left) and PC($^{13}\text{C}/*$) (Figure 4, top left) indicate direct electron-to-carbon polarization transfer. All of the ^{13}C centerbands of PC(*) show DNP enhancements but to varying degrees. The carbonyl-carbon peak is enhanced the most. The enhancement of the methyl-carbon peak at 30 ppm is negative. This enhancement was positive when the protons were irradiated by a string of 90° pulses during the microwave irradiation period (data not shown). The DNP-difference spectrum of PC($^{13}\text{C}/*$) obtained with 0.5-second microwave irradiation has relatively more of a broad component than the spectrum obtained with 2.0-second microwave irradiation (Figure 5, left). Based on the results of an inversion recovery experiment (Figure 5, right), the broad

component has a relatively long $T_1(C)$. Contributions from the carbons contributing to the broad component are almost completely dephased by the end of the second rotor period (*cf.*, below).

DNPFT-echo: The results of DNPFT-echo experiments performed on PC(*) and PC(^{13}C /*) also show direct electron-to-carbon polarization transfer (Figures 3 and 4, right). The vertical scaling of all six spectra of Figure 4 is the same allowing direct comparisons between the DNPFT and DNPFT-echo results on PC(^{13}C /*) to be made. The DNPFT-echo spectra have narrower lines with lower intensities relative to those obtained by the DNPFT experiment. The methyl-carbon peak of PC(*) shows a negative DNP enhancement in the echo spectra, which, because of the absence of broad resonances, is more obvious in the echo spectra than in the normal spectra. After one-second microwave irradiation, the DNP enhancements of resonances of the carbonyl carbon, protonated aromatic carbons, non-protonated aliphatic carbons, and methyl carbons are 7, 2, 3, and -1, respectively (Figure 3, left, middle, and top).

Synchronous Sampling: The first four synchronously sampled echoes for PC(^{13}C) and PC(^{13}C /*) are displayed as phase-independent magnitudes in Figure 6. The rotational-echo maxima for PC(^{13}C) under the chemical-shift interaction only decay with a time constant of 4.0 ms (Figure 6, top). The evolution of the magnetization for PC(^{13}C /*) under combined chemical-shift and C-H dipolar interactions is dephased within each rotor period and refocused at the end of a rotor period (Figure 6, middle). The resulting rotational-echo maxima decay with a time constant of 1.3 ms. The decay of

the echo maxima of the direct electron-to-carbon, DNP-enhanced magnetization for PC($^{13}\text{C}/^*$) under combined chemical-shift and C-H dipolar interactions has a time constant of 1.0 ms. The time constant of the decay of the echo train for PC($^{13}\text{C}/^*$) for chemical-shift interactions only was 2.1 ms (data not shown). The displays of the dephasing and refocusing of the first echo for PC(^{13}C) and PC($^{13}\text{C}/^*$) under combined chemical-shift and C-H dipolar interactions are expanded in Figure 7.

The Fourier transforms of the time-domain data of Figure 6 are asymmetrical about the centerband. Negative spinning sidebands appear at $n = -2$, and -3 for PC(^{13}C) (Figure 8, top) but not for PC($^{13}\text{C}/^*$) (Figure 9, top). All of the peaks in the PC($^{13}\text{C}/^*$) dipolar spectrum have DNP enhancements, with the natural-abundance ^{13}C non-protonated, aromatic-carbon peak enhanced the most (arrow, Figure 9, bottom). The enhanced peaks are superimposed on a broad resonance in the microwave-enhanced spectrum that appears to be shifted by about 1 kHz to low field (Figure 9, bottom).

The asymmetry of the dipolar sideband pattern for PC(^{13}C) differs from that for PC($^{13}\text{C}/^*$) (Figure 8) even though both samples have the same chemical shift anisotropy. The latter were measured by the ratio of the intensities of the first spinning sidebands to their respective centerbands (MAS = 1859 Hz) in an experiment in which the evolution of the magnetization was under chemical-shift interactions only (data not shown).

Simulations: Simulated spectra for carbon magnetization evolutions under chemical-shift interactions only, and under C-H dipolar interactions only, were adjusted to match the corresponding experimental results (Figure 10). The dipolar coupling and the principal components for the chemical-shift

tensor used in fitting the simulated spectra to the experimental spectra are presented in Table I. The experimental spectra were obtained under slow-spinning CPMAS and DRSE conditions, respectively. The parameters obtained from these fits were used to predict spectra obtained under CSA interactions only, and under combined CSA and C-H dipolar interactions at 1859-Hz magic-angle spinning (Figure 11, bottom). The asymmetry of the latter spectrum is pronounced even though the chemical-shift interaction is weak and the dipolar interaction symmetric.

Simulations that incorporate chemical-shift and C-H dipolar interactions assuming the applicability of a two-site jump model for the protonated, aromatic carbon match experimental 16-point stick spectra resulting from the Fourier transforms of synchronously-sampled carbon-magnetization evolution (Figure 12). For these transforms, $t = 0$ was defined by the top of the first echo after delayed H-H decoupling (see Figure 2) . The matches were best for two and three rotor-period delays with H-C decoupling.

DISCUSSION

Direct Electron-to-Carbon Polarization Transfer: The ^{13}C difference signals observed for PC(*) and PC($^{13}\text{C}/^*$) using the DNPFT and DNPFT-echo sequences (Figures 3 and 4) are proof of a direct electron-to-carbon polarization transfer. The ^{13}C resonances observed in the DNPFT-echo experiments are narrower than those observed in the DNPFT experiments. Carbons that are closer to the paramagnetic centers (electrons) are the first to be dephased by electron flips. These are also the carbons that are

polarized first (Figure 5, left) and the carbons with the longest $T_1(C)$ (Figure 5, right), the latter presumably the result of a combination of restrictions on motion imposed by the bulky free radical (III) and the selectivity of the DNP-enhancement process for sites with little spin-lattice leakage. We estimate that an electron-carbon dipolar broadening of 1500 Hz corresponds to a distance of 30 Å, and a broadening of 200 Hz corresponds to a distance of about 60 Å.

The DNP enhancement for the PC protonated, aromatic carbon under a direct electron-to-carbon transfer is about four (Figure 3, top). This is the same enhancement observed for the protons of PC and only one-fourth of the expected enhancement. The fast transfers to carbons occur over 30 Å which was probably not quite sufficient to span the irregular interface separating electrons and PC carbons in the thin-film PC/PS blends described in I. Slower transfers to more distant carbons which have narrower, more easily detected lines, must still compete with the leakage due to fast ^{13}C spin-lattice relaxation. This combination explains the failure to detect an interface-PC echo signal after two rotor periods by direct electron-to-carbon transfer as reported in I and II.

Three-Spin Effect: The chemically different carbons of PC(*) have varying DNP enhancements (Figure 3) reflecting differences in their T_1 's and DNP leakage factors. The enhancement of the carbonyl-carbon peak at 150 ppm is about three times that of the other carbons, consistent with the carbonyl-carbon T_1 of 10 seconds [2], compared to T_1 's of about 0.1 and 0.2 seconds for the methyl carbons and the protonated, aromatic carbons, respectively [3].

The negative DNP enhancement of the methyl carbons is due to a *three-spin effect*, first observed in solution DNP NMR studies of electron-proton-carbon coupling [4] and electron-proton-fluorine coupling [5,6], and more recently in solids DNP NMR studies of electron-proton-carbon coupling [7]. The three-spin effect is observed in cases where one of two nuclei is more strongly polarized by the electrons than the other, and the two kinds of nuclear spins are strongly coupled to each other. Theoretical descriptions of the three-spin effect may be found in references 4 and 8. The microwave irradiation at the difference of the electron and carbon Larmor frequencies is sufficiently close to resonance for the electrons that protons can be polarized by an Overhauser DNP effect, assuming the presence of fast molecular motion. Only the methyl-carbon resonance has a negative DNP enhancement because of the short correlation time of the internal methyl-carbon C_3 rotation. When the protons of PC(*) were saturated by a string of uniformly-spaced proton 90° pulses during the microwave-irradiation period, all of the ^{13}C DNP enhancements were positive, proving that the negative DNP enhancement is indeed due to a three-spin Overhauser effect. Similar results have been reported by G.G. Maresch *et al* [9] on other polymer systems.

Synchronous Sampling and Asymmetrical Sideband Patterns: The spinning sidebands observed for PC(^{13}C) and PC($^{13}C/^{*}$) in the synchronous-sampling experiments under chemical-shift interactions only (C-H dipolar interactions decoupled) are small compared to the centerbands because of the small chemical shift anisotropies at the relatively low field of 1.4 T. The ratio of the intensities of the first sidebands to the centerband is 4% or less in both PC(^{13}C) and PC($^{13}C/^{*}$) spectra. In H-H multiple-pulse decoupled

synchronous sampling, an asymmetrical pattern is expected because the effect on evolution of the chemical-shift tensor is included. The synchronous-detection experiments were performed with no chemical-shift selectivity. Each time-domain data point represents all carbons regardless of their chemical-shift tensor or offset. Although the major contributor to the spectra of Figures 8 and 9 is the ^{13}C -enriched, protonated, aromatic carbon, all other carbons make contributions.

The simulated spectrum obtained under the combined CSA and C-H dipolar interactions *qualitatively* agrees with the spectrum obtained experimentally (Figure 8), in that the experimental and simulated spectra are asymmetric about the centerband. But the details do not match: for example, both $n=2$ and $n=-2$ sidebands of the simulated spectrum are more intense than the centerband (Figure 11, bottom), while the experiment shows an intense $n=2$ sideband, but a negative-going $n=-2$ sideband for PC(^{13}C) (Figure 8, top). Negative sidebands can result from incomplete powder averaging, but in our case the evolution occurred over complete rotor periods and negative sidebands are not expected. We believe that the negative sidebands could be due to intermolecular ^{13}C - ^{13}C interactions that do not refocus at the rotor period. In addition, contributions from non-protonated aromatic carbons are possible. The non-protonated, aromatic-carbon peaks are frequency offset with respect to the protonated, ^{13}C -labeled, aromatic-carbon resonances. The offsets could accumulate phase to create the appearance of negative sidebands. The shifted broad line (Figure 8, bottom) may indicate an isotropic shift arising from specific orientations of PC chains closest to BDPA.

The delayed H-H decoupling sequence of Figure 2 selects carbons distant from the free-radical centers. Most of the carbons that are close to

BDPA are dephased by the end of the second rotor period as shown by the decrease in the intensity of the broad component in Figure 4. Stick spectra obtained by Fourier transforms of 16 time-domain points from delayed data acquisition match simulations that incorporate chemical-shift and C-H dipolar interactions *and* two-site jumps of the phenyl rings (Figure 12). The spectra were obtained from the time-domain data collected after two and three rotor-period delays in the MREV-8 multiple-pulse decoupling. A simulated spectrum with 75% of the sites undergoing two-site ring flips matches the stick spectrum after a two rotor-period delay in the H-H multiple-pulse decoupling. The simulated spectrum with all sites undergoing two-site jumps (as in bulk PC) matches the experimental spectrum after a delay of three rotor periods in the MREV-8 decoupling. The match between experiment and simulation should be considered *qualitative* because intermediate-frequency motions that affect the lineshape are not represented in the simulations. Nevertheless, we conclude that a narrow carbon resonance is a guarantee of sufficient distance from BDPA that molecular dynamics are not affected. Thus the conclusions about PC dynamics at interfaces reported in III are free from complications due to distant BDPA in PS.

Time-Domain Analysis: The time-domain data shows that the BDPA-doped PC has echoes that both form and are dephased faster than echoes in PC (Figure 7). Doped PC therefore has a broader distribution of sidebands in the dipolar frequency domain. A broader distribution of sidebands in the dipolar domain means that BDPA-doped PC has more restricted motion; that is, PC chains are less mobile in the presence of BDPA. Presumably the bulk of BDPA affects chain packing and disrupts coordinated PC chain

motion. In other words, BDPA acts as an antiplasticizer [10]. We believe that the broadening of the distribution of sidebands is not the result of electron flips, which are on a msec time scale, interfering with the efficiency of the MREV-8 decoupling because of the symmetry of the PC($^{13}\text{C}/^*$) echo near its center (Figure 7).

CONCLUSION

In these four papers we have demonstrated the practicality of using 50-Å, direct electron-nuclear polarization transfers for both selectivity and sensitivity in characterizing the interfaces of immiscible, amorphous polymers by NMR. The double thin-film technique for doping one component of an immiscible blend with a non-covalently bound stable free radical is general, so long as a solvent-nonsolvent pair can be found for the two polymers of the blend. When chemical-shift differences between doped and undoped polymers are not large, stable-isotope labeling can be used to distinguish components. Once the polarization transfer has been made, standard NMR relaxation experiments measure the microscopic motions of those chains in the undoped phase which are at the interface, with no interferences from the free radical. The results obtained so far for a model of the commercially important blend of polycarbonate and polystyrene indicate that polycarbonate chains near the interface are immobilized, probably the result of local, atypical variations in packing density. It remains for future studies to examine this packing as a function of thermal history and exposure to solvents and compatibilizers to connect

the mechanical properties of the blend with structure and dynamics of chains at the interface.

ACKNOWLEDGEMENTS

This work has been supported by the Office of Naval Research under contract N00014-88-K-0183.

Table I Parameters for Simulations

	σ_{xx}	σ_{yy}	σ_{zz}	D_{CH}	<u>MAS</u>	<u>flip angle</u>
	(kHz)			(kHz)	(kHz)	
<i>CSA only</i>	0.300	1.100	-1.400	--	0.600	---
<i>CSA only</i>	0.300	1.100	-1.400	--	1.859	---
<i>CSA plus C-H dipolar</i>	0.300	1.100	-1.400	9.0	1.859	---
<i>C-H dipolar only</i>	---	---	---	9.0	1.859	---
<i>CSA plus C-H dipolar with two-site jumps</i>	0.300	1.100	-1.400	9.0	1.859	180°

REFERENCES

1. Olejniczak, E.T.; Vega, S.; Griffin, R.G. *J. Chem. Phys.*, **1984**, *81*, 4804.
2. Henrichs, P.M.; Linder, M.; Hewitt, J.M.; Massa, D.; Isaacson, H.V. *Macromolecules*, **1984**, *17*, 2412.
3. Walton, J.H.; Lizak, M.J.; Conradi, M.S.; Gullion, T.; Schaefer, J. *Macromolecules*, **1990**, *23*, 416.
4. Hausser, K.H.; Reinbold, F. *Phys. Lett.*, **1962**, *2*, 53.
5. Richards, R.E.; White, J.W. *Proc. Chem. Soc.*, **1962**, p. 119.
6. Richards, R.E.; White, J.W. *Disc. Faraday Soc.*, **1962**, *34*, 96.
7. Duijvestijn, M.J.; Wind, R.A.; Smidt, J. *Physica*, **1986**, *138B*, 147 (and references therein).
8. Natusch, D.F.S.; Richards, R.E.; Taylor, D. *Mol. Phys.*, **1966**, *11*, 421.
9. Maresch, G.G.; Kendrick, R.D.; Yannoni, C.S.; Galvin, M.E. *J Magn. Reson.*, **1989**, *82*, 41.
10. Wehrle, M; Hellmann, G.P.; Spiess, H.W. *Colloid and Poly. Sci.*, **1987**, *265*, 815

FIGURE CAPTIONS

Figure 1. Pulse sequences for synchronous sampling data acquisition. A 5.0- μs 90° inspection pulse on the carbon channel is followed by data acquisition every 33.6 μs with either full C-H decoupling at 87 kHz (top) or multiple-pulse H-H decoupling (bottom). The one-point detections, represented by dots in the figure, are synchronized both with the cycle time of the semi-windowless MREV-8 sequence ($t_c = 33.6 \mu\text{s}$), and the rotor period ($16 \times 33.6 \mu\text{s} = 538 \mu\text{s}$). The ^{13}C inspection pulse is preceded by a one rotor-period preparation period.

Figure 2. Pulse sequence for delayed MREV-8 decoupling and synchronous detection. The experiment begins with a ^{13}C inspection pulse followed by C-H decoupling for an integral number of rotor periods. The magnetization is then allowed to evolve under combined chemical-shift and C-H dipolar interactions. Synchronous sampling (solid circles) is performed with H-H interactions suppressed by semi-windowless MREV-8 multiple-pulse decoupling. The nT_R delay selects carbons that are distant from the free-radical centers.

Figure 3. 15.1-MHz DNPFT and DNPFT-echo ^{13}C NMR spectra of PC(*) following direct electron-to-carbon polarization transfer. The spectra on the left are the result of a DNPFT experiment with (bottom) and without (middle) one-second microwave irradiation. The spectra on the right are the result of a DNPFT-echo experiment with (bottom) and without (middle) one-second microwave irradiation. The top spectra are differences (bottom minus middle). In both experiments the methyl-carbon peak at 30 ppm

shows a negative DNP enhancement due to an electron-proton-carbon *three-spin effect*.

Figure 4. 15.1-MHz DNPFT and DNPFT-echo ^{13}C NMR spectra of $\text{PC}(^{13}\text{C}/^*)$ following direct electron-to-carbon polarization transfer. The spectra on the left are the result of a DNPFT experiment with (bottom) and without (middle) one-second microwave irradiation. The spectra on the right are the result of a DNPFT-echo experiment with (bottom) and without (middle) one-second microwave irradiation. The top spectra are differences (bottom minus middle). In both cases a total of 2064 scans were averaged. The vertical display scale for all six spectra is the same.

Figure 5. (Left) DNPFT ^{13}C NMR *difference* spectra of $\text{PC}(^{13}\text{C}/^*)$ with 0.5 and 2.0-second microwave irradiation at the difference of the electron and *carbon* Larmor frequencies. The experiments were done as an alternate-block, add-subtract, equal-heat acquisition with all relaxation delays balanced. The difference spectra were generated by averaging 2000 scans in each of the two blocks. (Right) DNPFT ^{13}C NMR difference spectrum 800 mseconds after a 180° ^{13}C inversion pulse.

Figure 6. The magnitudes of PC rotational echoes acquired synchronously using the pulse sequences shown in Figure 1. The evolution of the carbon magnetization was measured under chemical-shift interactions only (top), and under combined chemical-shift and C-H dipolar interactions with H-H interactions decoupled by semi-windowless MREV-8 multiple-pulse decoupling (middle and bottom) for $\text{PC}(^{13}\text{C})$ (top and middle) and $\text{PC}(^{13}\text{C}/^*)$ (bottom). Only 64 of 256 data points acquired are shown with the first five

data points removed. Most of the signal has disappeared by $2T_R$ for the BDPA-doped PC.

Figure 7. The first echo for PC(^{13}C) and PC($^{13}\text{C}/^*$) with evolution under combined chemical-shift and C-H dipolar interactions. The formation and dephasing for the free-radical doped sample are faster than those for the undoped sample. Data points are connected by solid and dotted lines to guide the eye.

Figure 8. Fourier transforms of the time-domain data shown in Figure 6 (middle and bottom) with $t = 0$ defined by the top of the first echo.

Figure 9. Fourier transforms of the time-domain data of the synchronous-acquisition experiments of Figure 1 on PC($^{13}\text{C}/^*$) with (bottom) and without (top) one-second microwave irradiation. The microwave irradiation was followed by a one rotor-period preparation with MREV-8 decoupling prior to the ^{13}C inspection pulse. The Fourier transform was performed with $t=0$ defined by the top of the first echo by left shifting the first 16 points, zero filling to 1-K data points, and imposing a 20-Hz line broadening. The natural-abundance ^{13}C non-protonated, aromatic-carbon line is strongly enhanced (arrow). This spectrum also appears at the bottom of Figure 8. A total of 37,000 scans were collected to generate each spectrum.

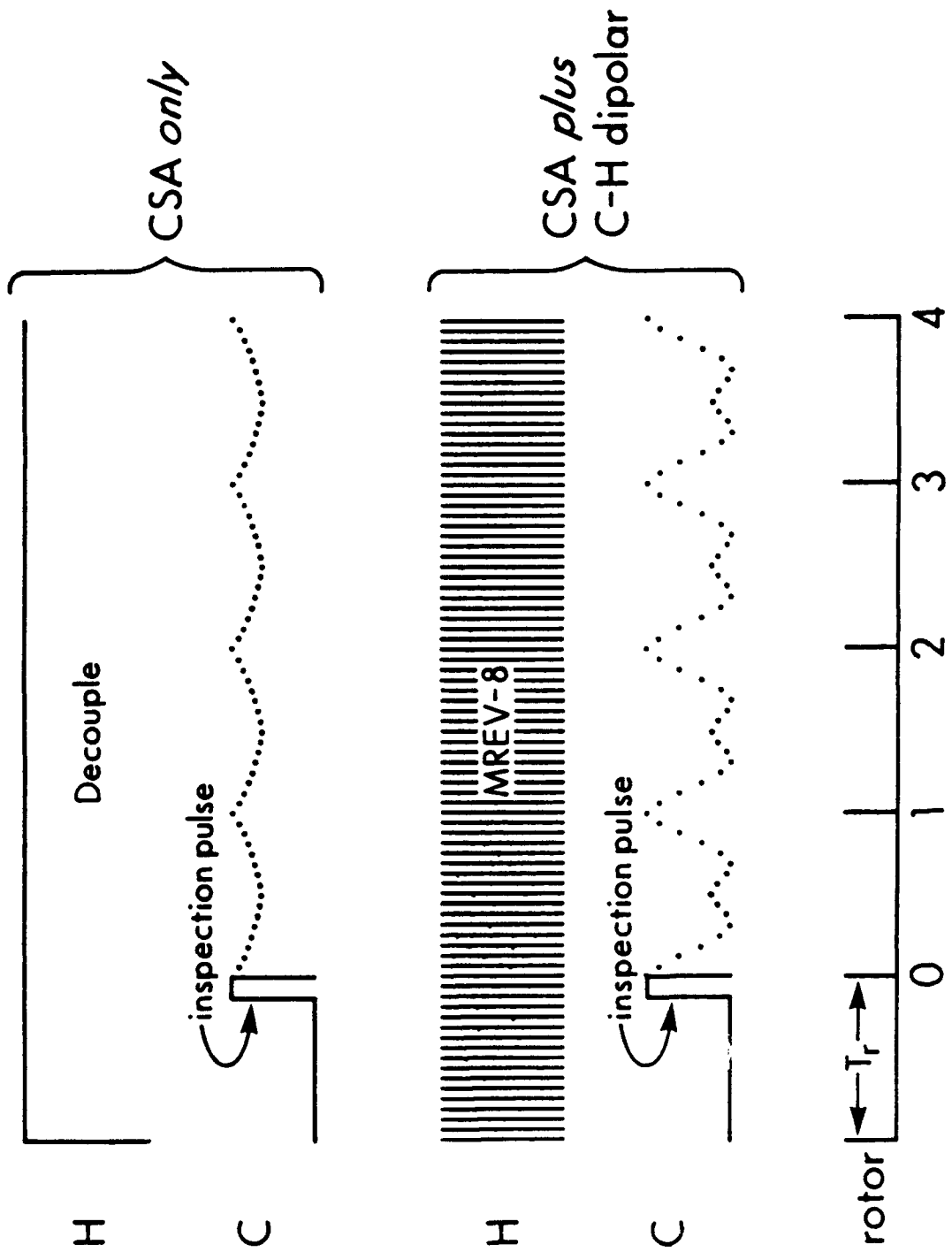
Figure 10. Experimental and simulated spectra of the protonated, aromatic-carbon magnetization of PC under chemical-shift interactions *only* (left) and under C-H dipolar interactions *only* (right). The calculated fit to the dipolar spectrum is only approximate because the effects of non-flip

motions were not included. The parameters used in the simulations are given in Table I.

Figure 11. Simulations of sideband patterns for protonated, aromatic-carbon magnetization with chemical-shift interactions *only* (top) and combined chemical-shift *plus* C-H dipolar interactions under magic-angle spinning at 1859 Hz. The asymmetries in the patterns arise from the anisotropic chemical shift.

Figure 12. Experimental and simulated spectra of the protonated, aromatic-carbon magnetization of PC($^{13}\text{C}/^*$). The experimental spectra are the results of a delayed-decoupling experiment (Figure 2) after two (top left) and three (top right) rotor-periods of C-H decoupling following the inspection pulse. The bottom two spectra are simulations with chemical-shift and C-H dipolar interactions assuming a two-site jump model for ring flips in which only 75% of the rings flip (bottom left) and all rings flip (bottom right).

Figure 1



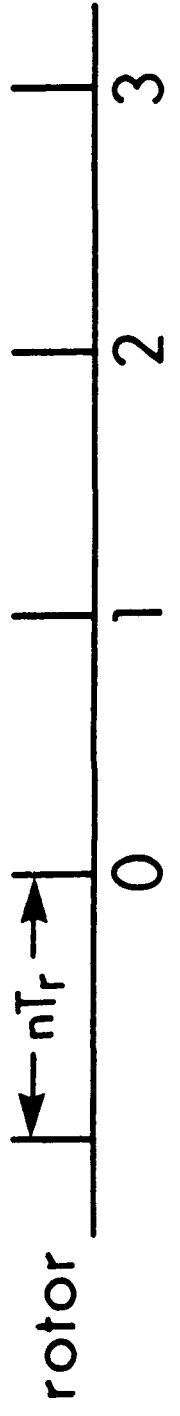
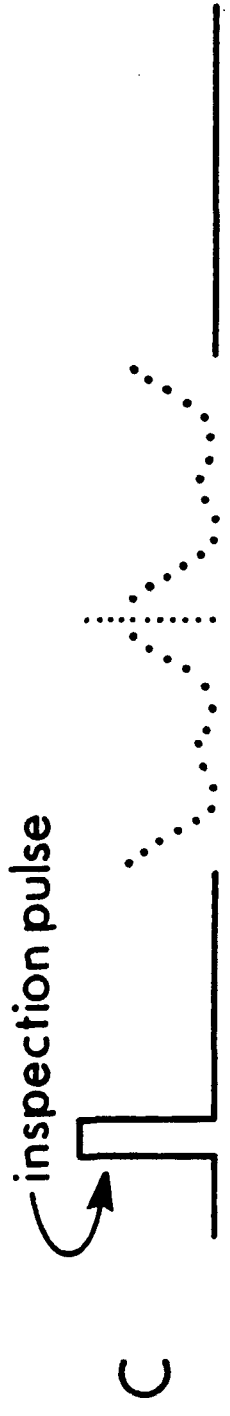
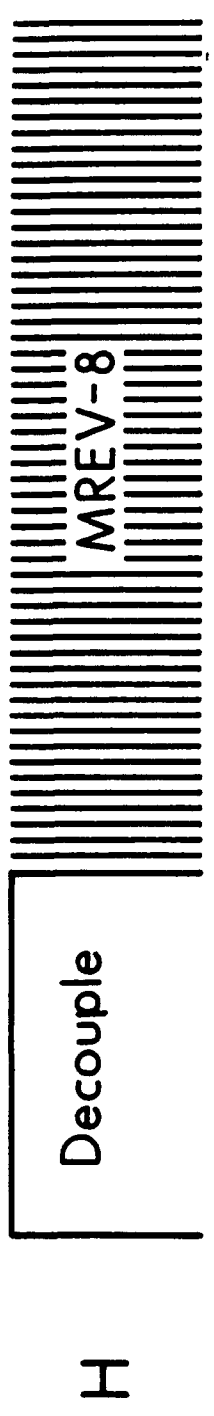


Figure 2

DNP of PC(*)
Electrons to Carbons Directly

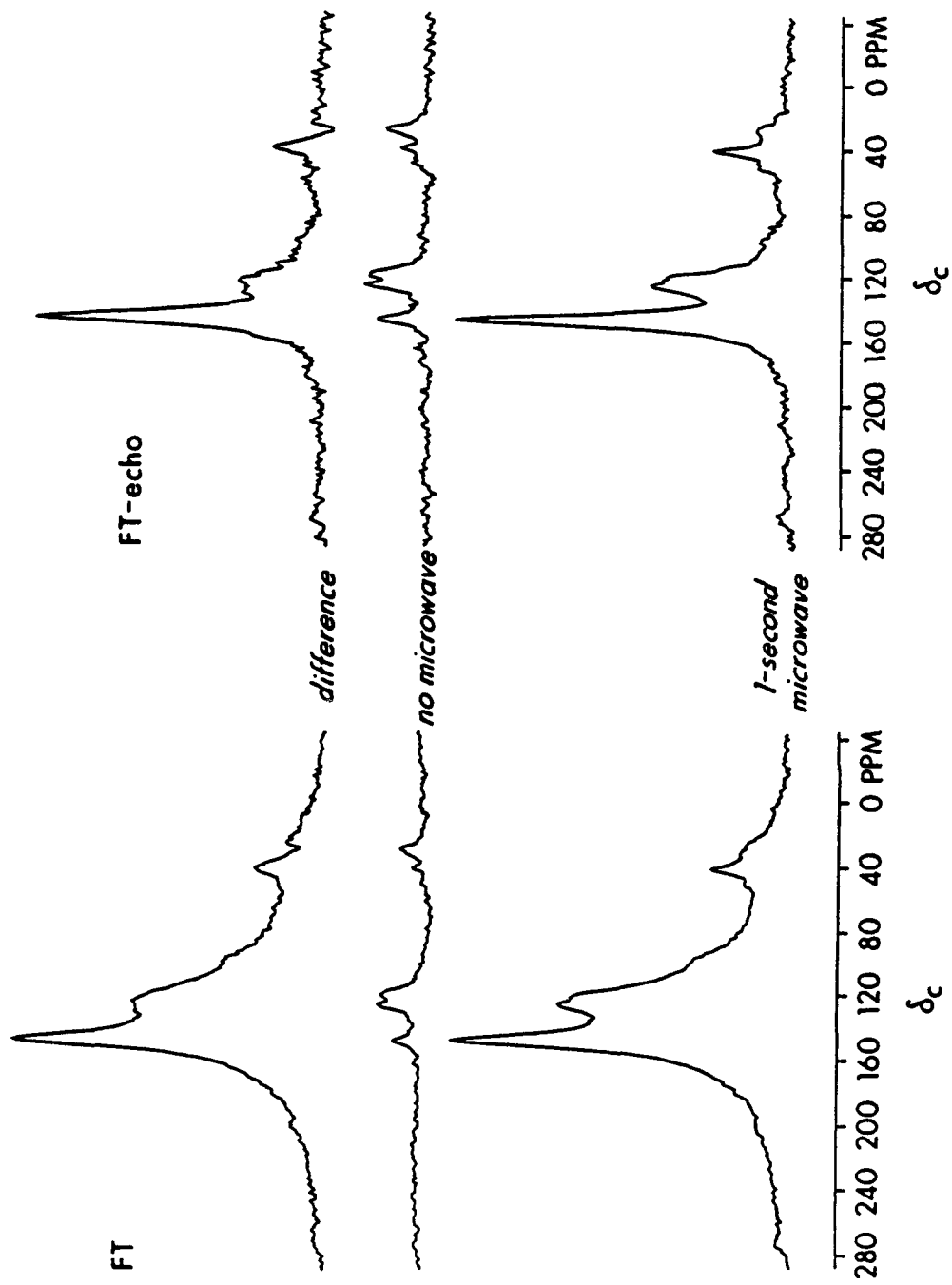


Figure 3

DNP of PC ($^{13}\text{C}/*$)
Electrons to Carbons Directly

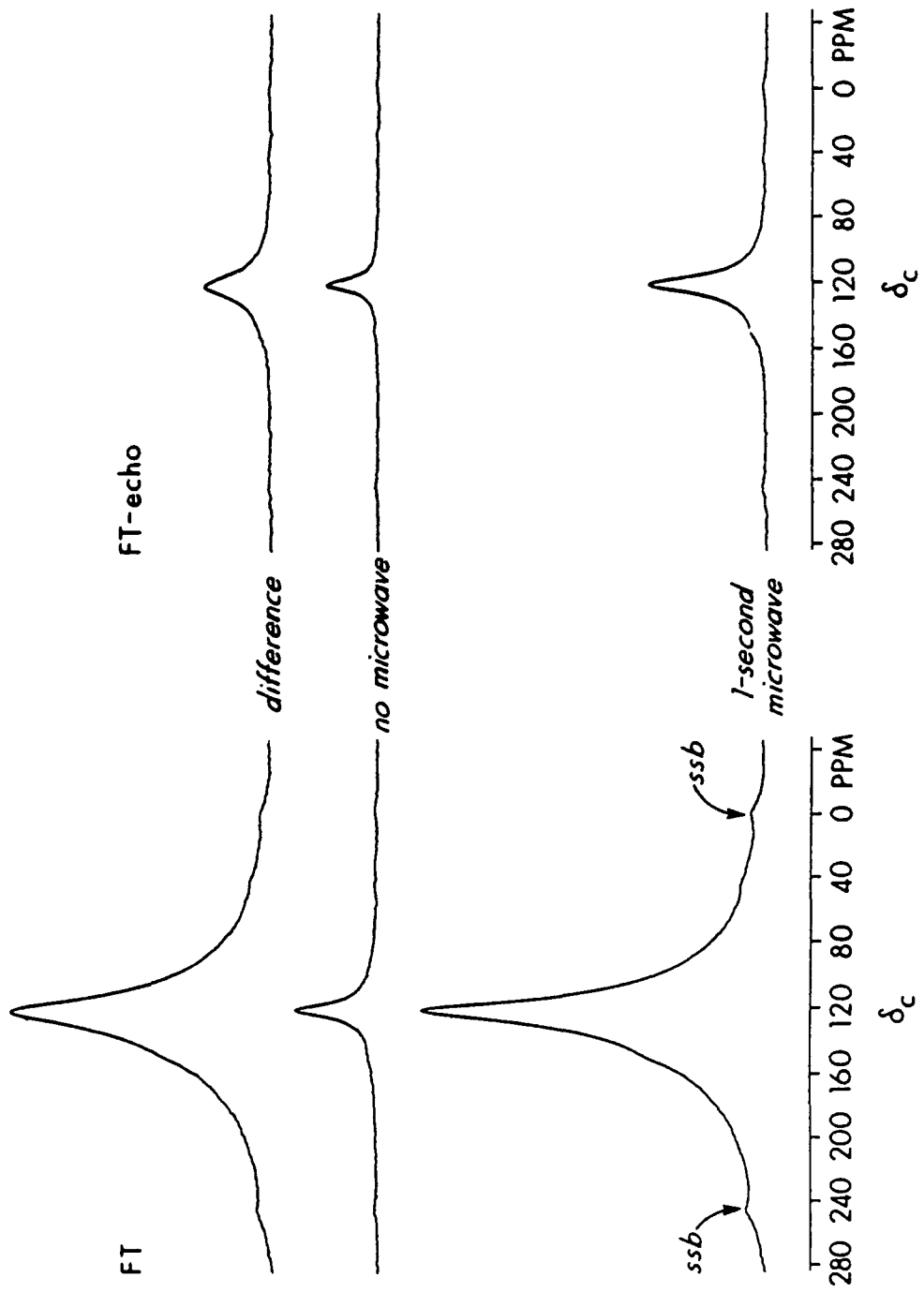
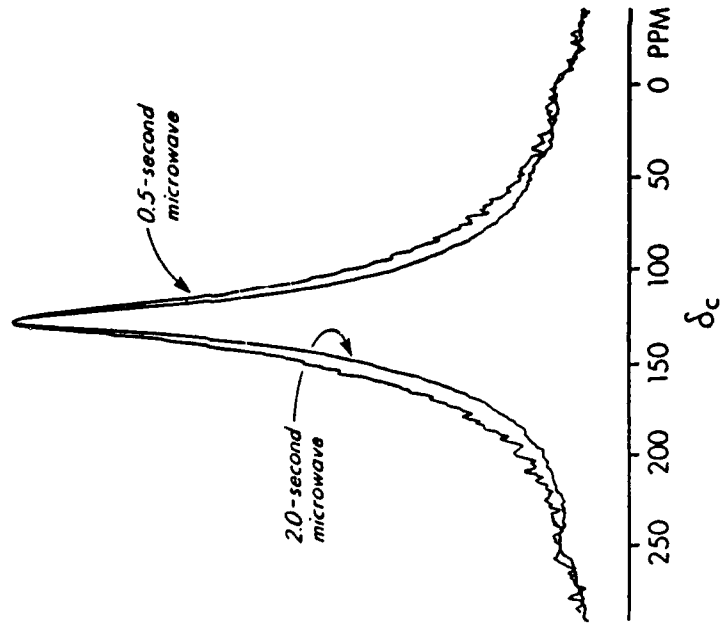


Figure 4

DNP DIFFERENCE OF PC($^{13}\text{C}/*$)
Electrons to Carbons Directly



**0.8 Seconds after Inversion Following
2.0-Second Microwave Pumping**

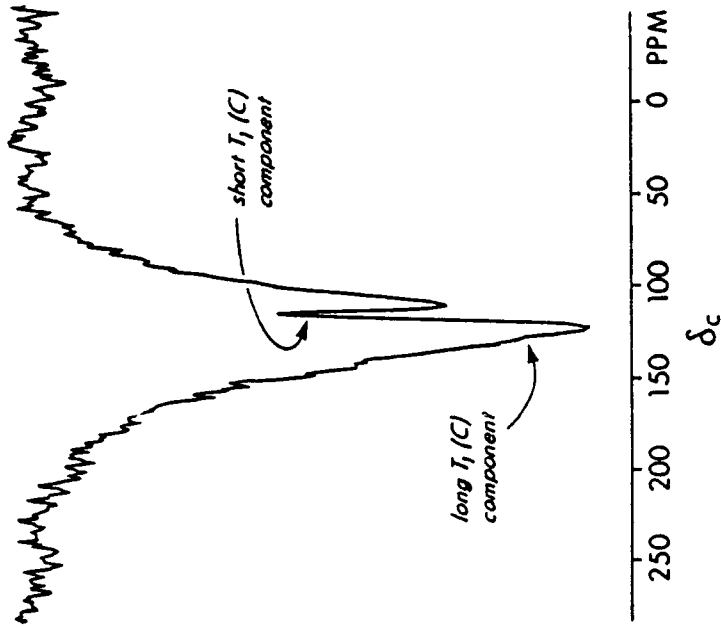


Figure 5

POLYCARBONATE ROTATIONAL ECHOES

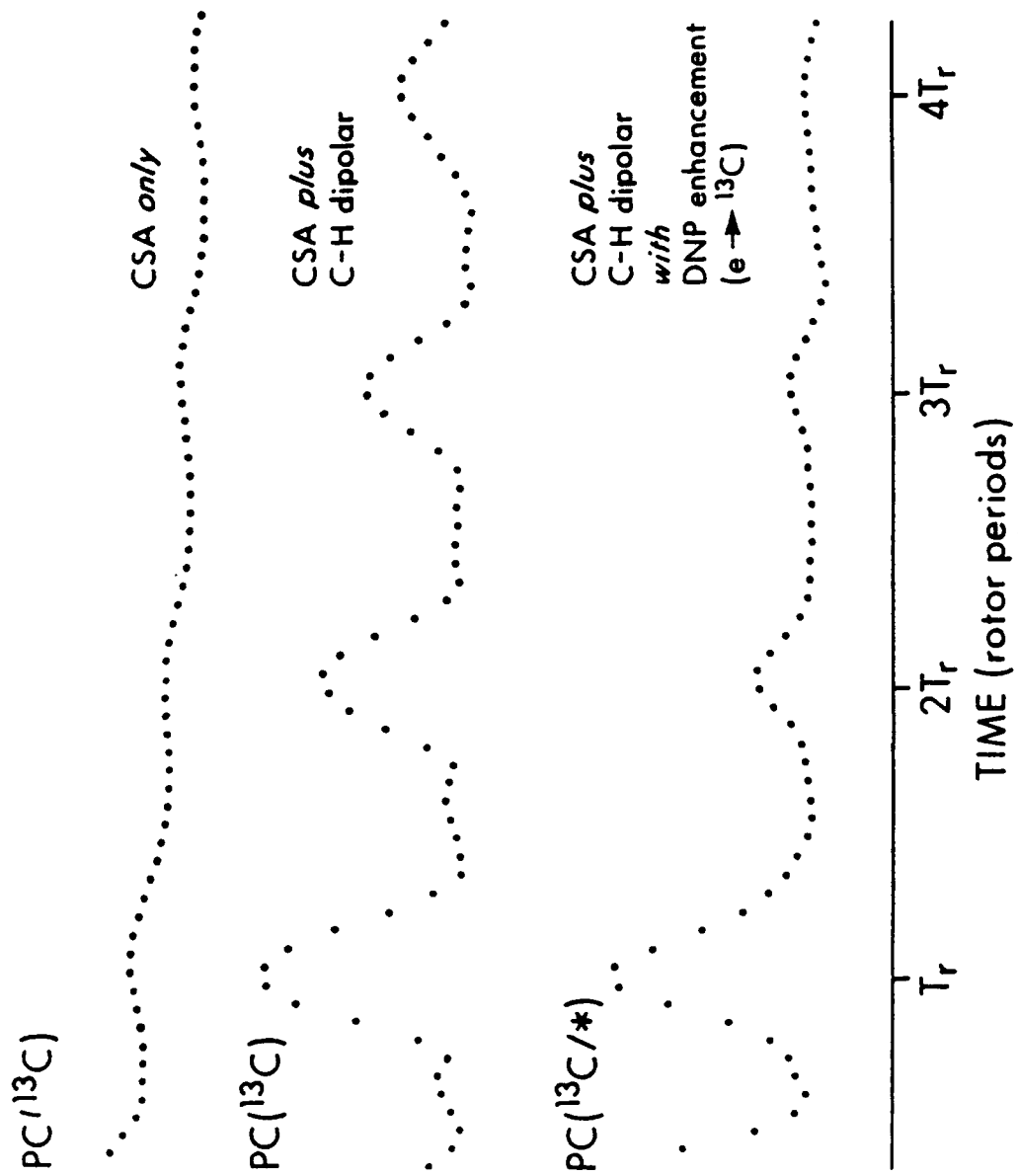


Figure 6

POLYCARBONATE with MREV-8 Decoupling

first rotational echo

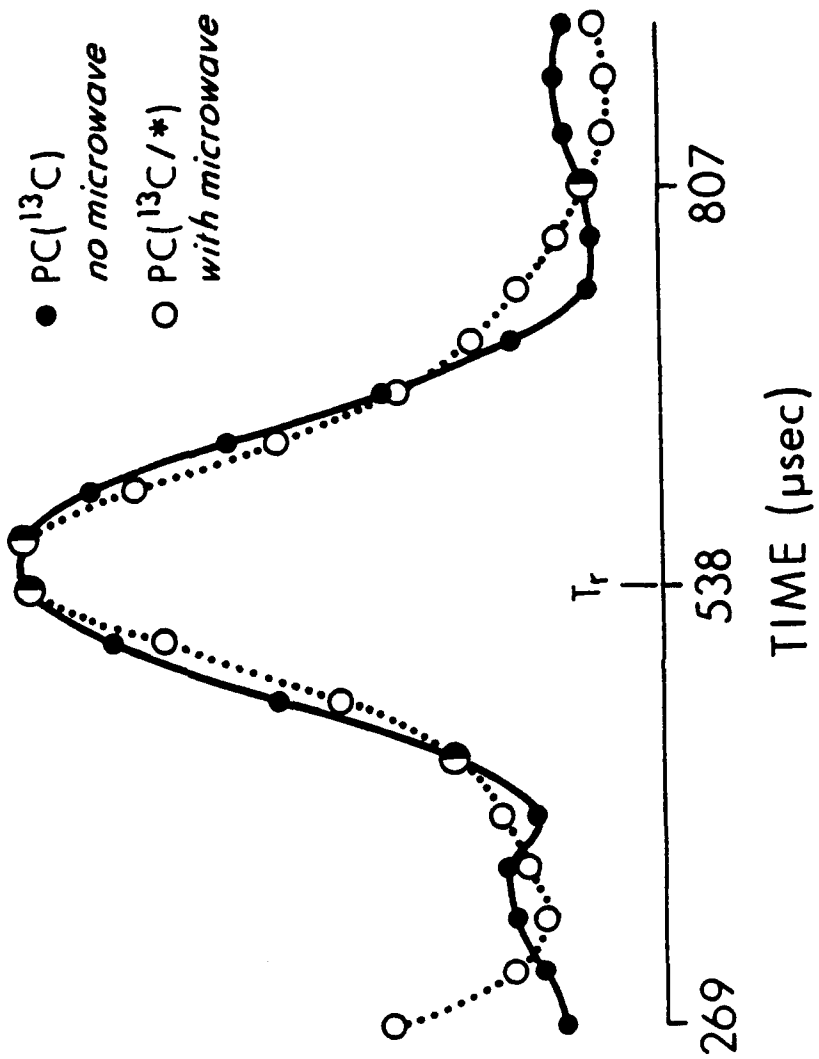
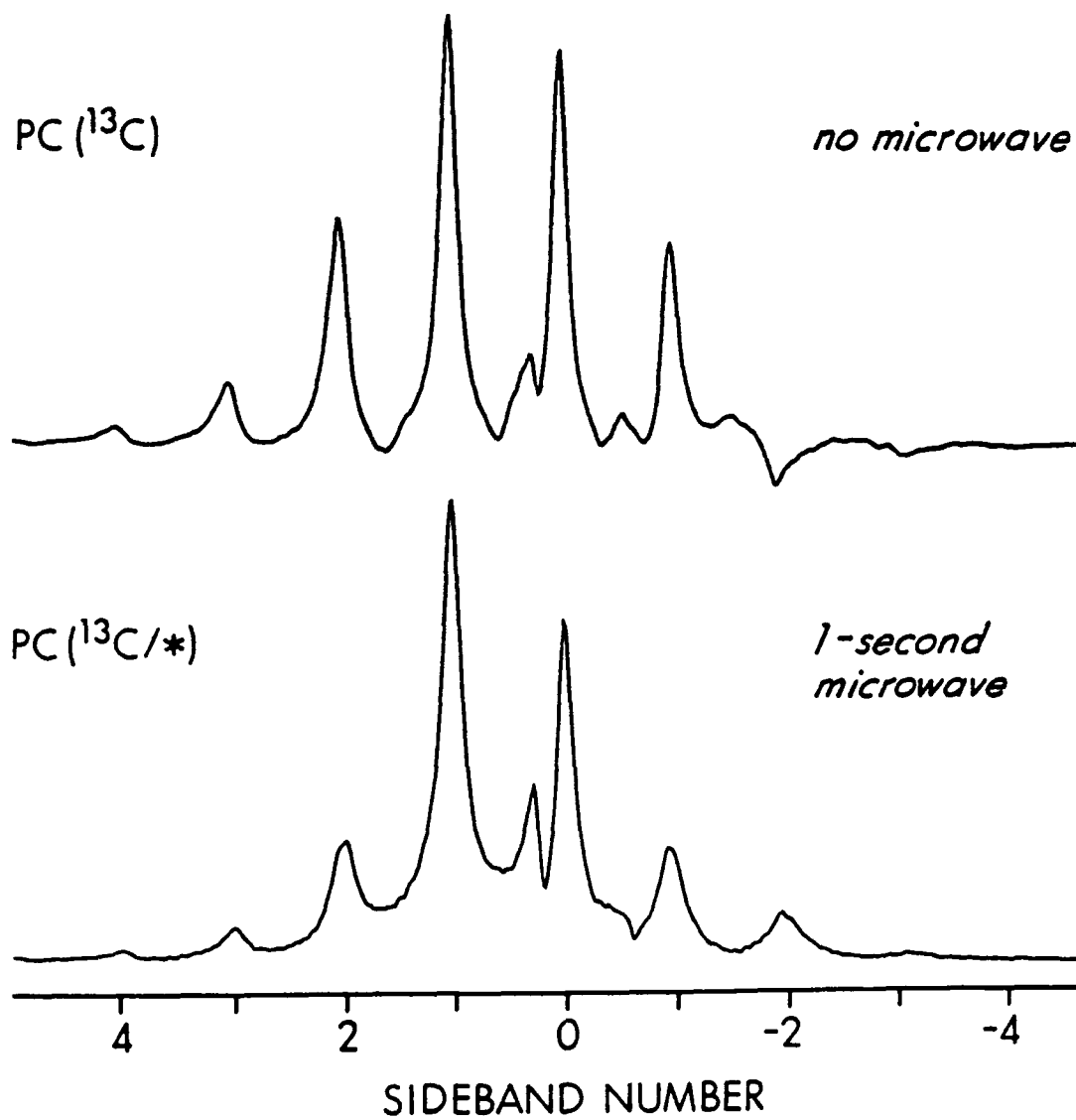


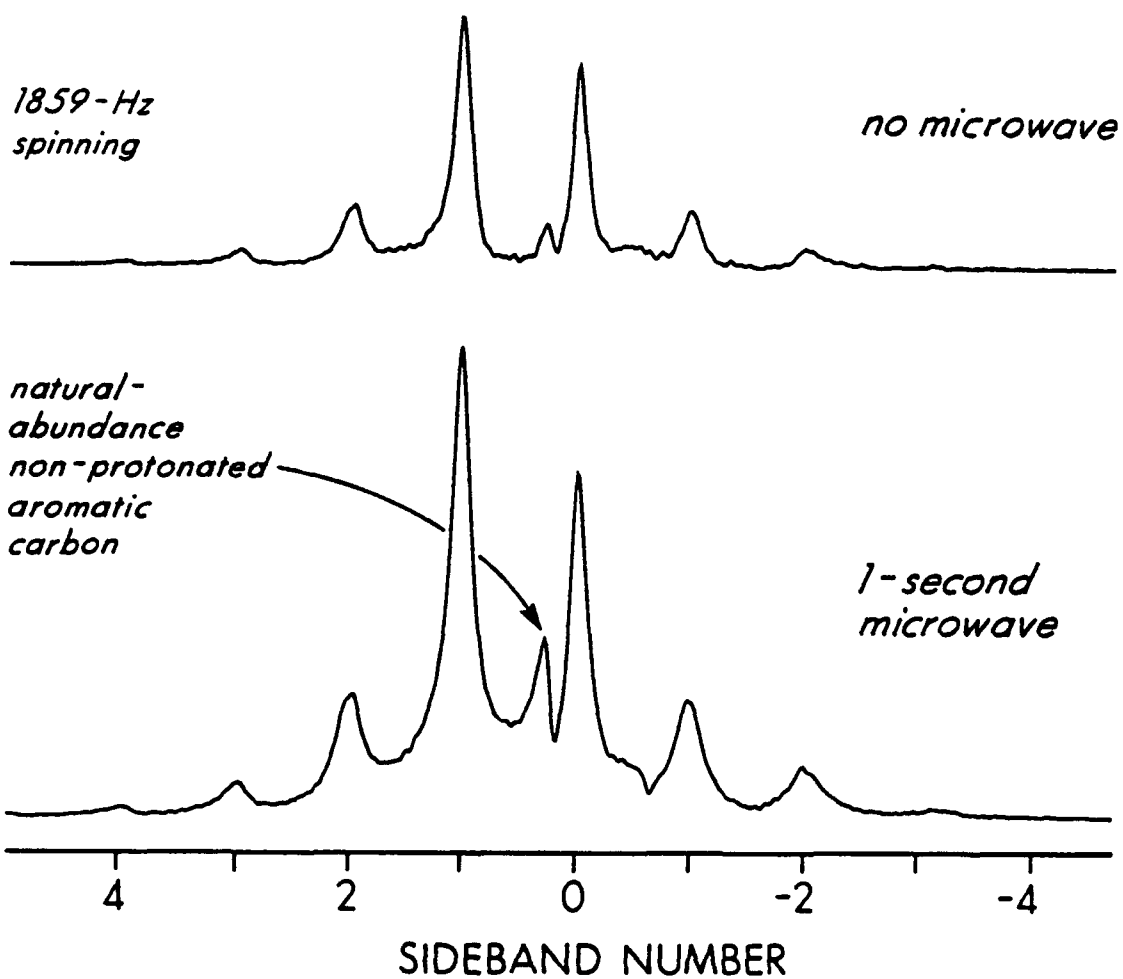
Figure 7

DNP with MREV-8 Decoupling
Electrons to Carbons Directly

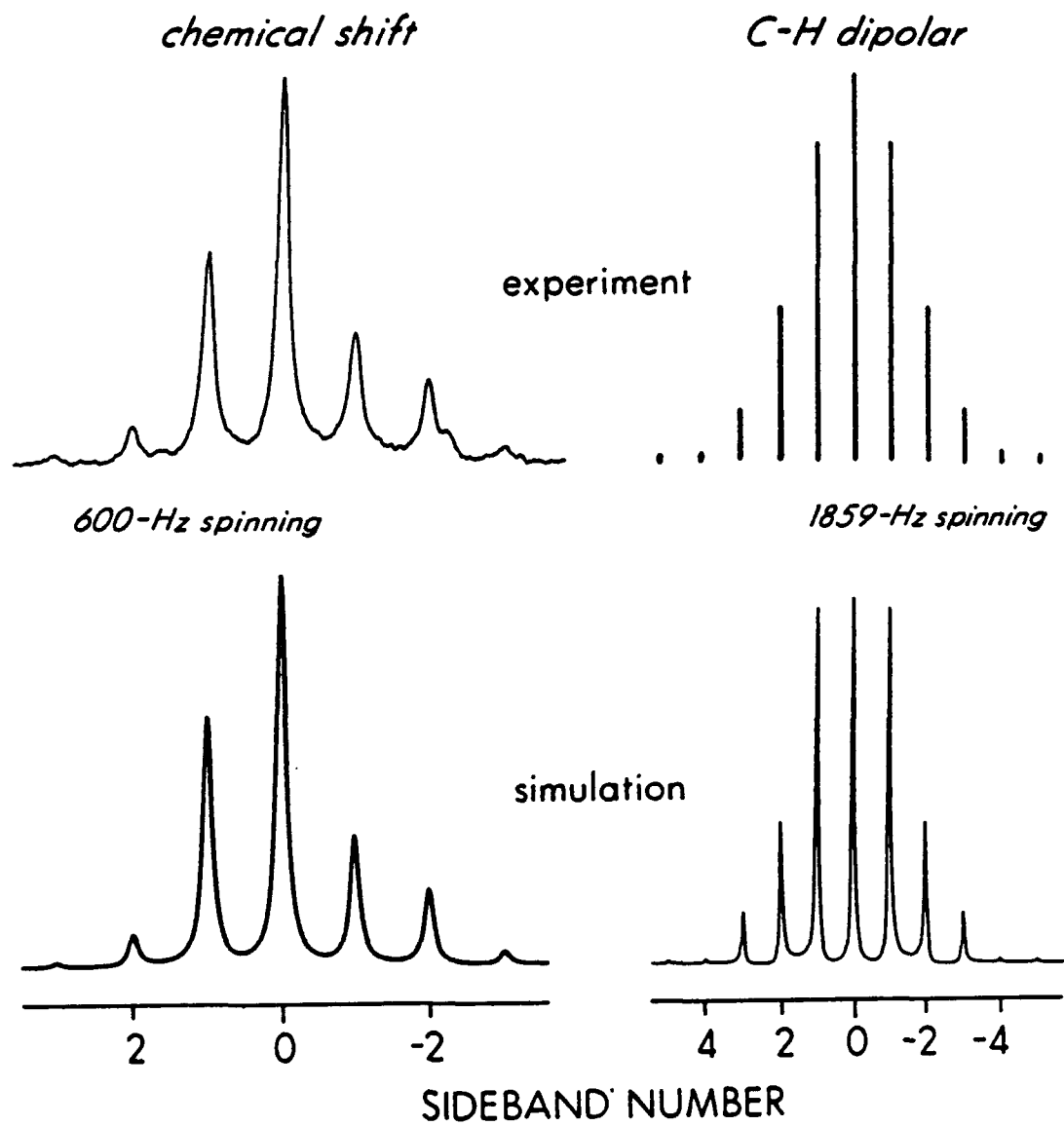


DNP of PC ($^{13}\text{C}/*$) with MREV-8 Decoupling

Electrons to Carbons Directly

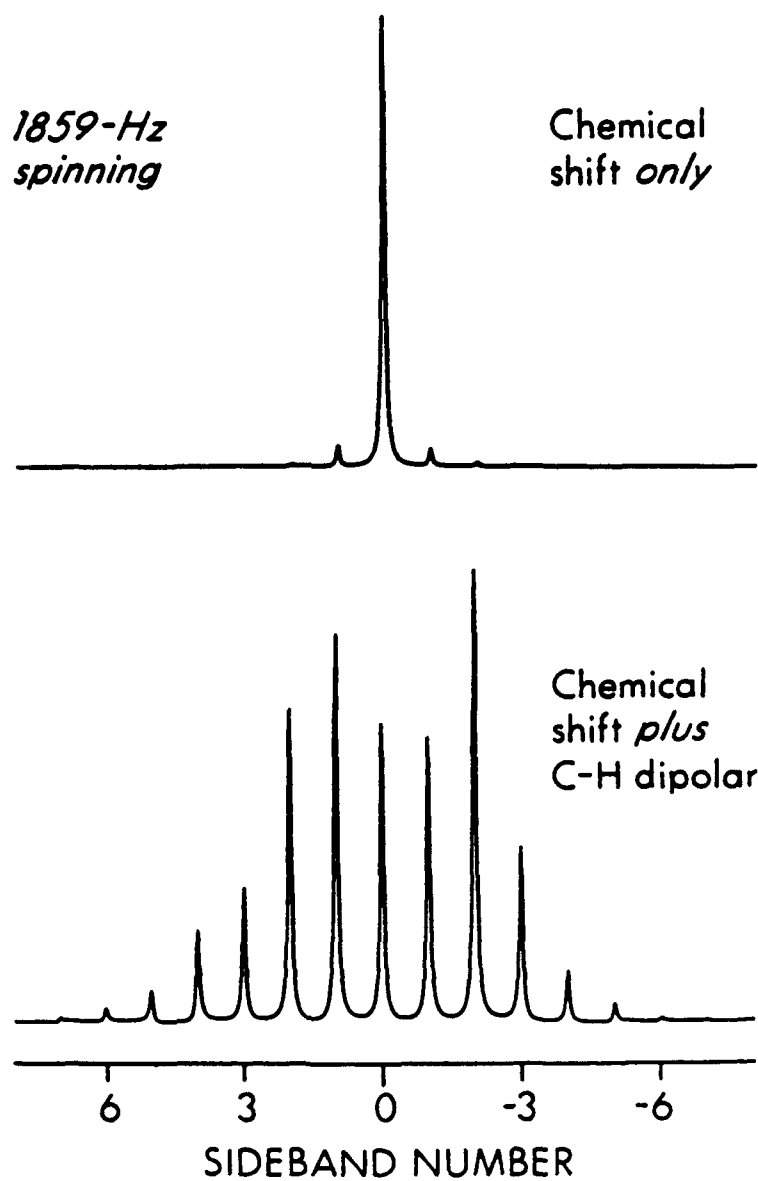


POLYCARBONATE AROMATIC CARBON



POLYCARBONATE AROMATIC-CARBON SIMULATIONS

Low Field and Fast Spinning



PC($^{13}\text{C}/*$) with MREV-8 Decoupling

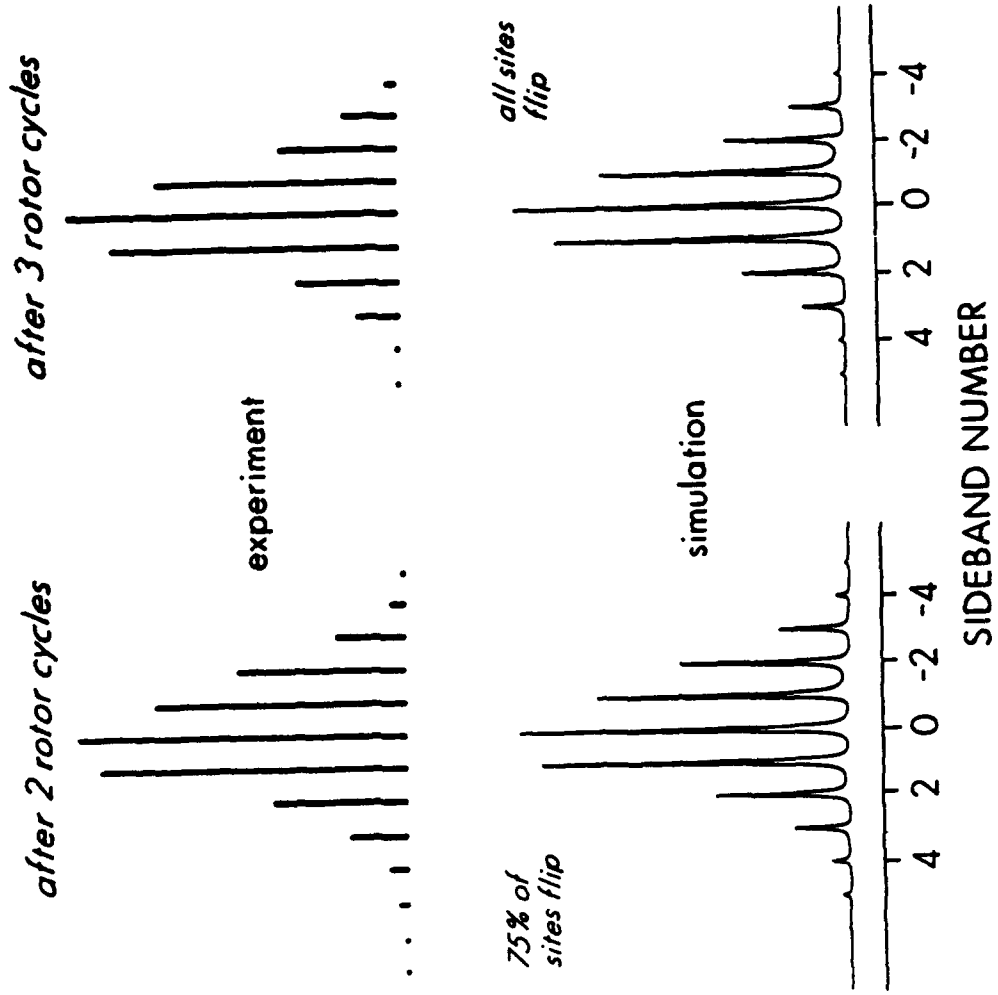


Figure 12

TECHNICAL REPORT DISTRIBUTION LIST - GENERAL

Office of Naval Research (2)
Chemistry Division, Code 1113
800 North Quincy Street
Arlington, Virginia 22217-5000

Commanding Officer (1)
Naval Weapons Support Center
Dr. Bernard E. Douda
Crane, Indiana 47522-5050

Dr. Richard W. Drisko (1)
Naval Civil Engineering
Laboratory
Code L52
Port Hueneme, CA 93043

David Taylor Research Center (1)
Dr. Eugene C. Fischer
Annapolis, MD 21402-5067

Dr. James S. Murday (1)
Chemistry Division, Code 6100
Naval Research Laboratory
Washington, D.C. 20375-5000

Dr. Robert Green, Director (1)
Chemistry Division, Code 385
Naval Weapons Center
China Lake, CA 93555-6001

Chief of Naval Research (1)
Special Assistant for Marine
Corps Matters
Code 00MC
800 North Quincy Street
Arlington, VA 22217-5000

Dr. Bernadette Eichinger (1)
Naval Ship Systems Engineering
Station
Code 053
Philadelphia Naval Base
Philadelphia, PA 19112

Dr. Sachio Yamamoto (1)
Naval Ocean Systems Center
Code 52
San Diego, CA 92152-5000

Dr. Harold H. Singerman (1)
David Taylor Research Center
Code 283
Annapolis, MD 21402-5067

In preparing the general distribution list for the TECHNICAL REPORTS, the address for the Defense Technical Information Center (DTIC) was omitted. When technical reports are prepared, two high quality copies should be forwarded to:

Defense Technical Information Center
Building 5, Cameron Station
Alexandria, VA 22314

(2)